Biochimica et Biophysica Acta 1818 (2012) 2302–2313

Contents lists available at SciVerse ScienceDirect

Biochimica et Biophysica Acta

journal homepage: www.elsevier.com/locate/bbamem

Binding of the three-repeat domain of tau to phospholipid membranes induces an aggregated-like state of the protein

Georg Künze[a], Patrick Barré[b,c], Holger A. Scheidt[a], Lars Thomas[a], David Eliezer[b], Daniel Huster[a,*]

[a] Institute of Medical Physics and Biophysics, University of Leipzig, Härtelstrasse 16-18, D-04107 Leipzig, Germany
[b] Department of Biochemistry and Program in Structural Biology, Weill Cornell Medical College of Cornell University, 1300 York Avenue, New York, NY 10021, USA
[c] IMR Laboratory, UPR 3243, Institut de Microbiologie de la Méditérannée, CNRS and Aix-Marseille Universités, 31 Chemin Joseph Aiguier, 13402 Marseille Cedex 20, France

ARTICLE INFO

Article history:
Received 9 December 2011
Received in revised form 28 March 2012
Accepted 29 March 2012
Available online 6 April 2012

Keywords:
Tau
Alzheimer's disease
Phospholipid
Membrane
Protein aggregation

ABSTRACT

In patients with Alzheimer's disease, the microtubule-associated protein tau is found aggregated into paired helical filaments (PHFs) in neurofibrillary deposits. In solution, tau is intrinsically unstructured. However, the tubulin binding domain consisting of three or four 31–32 amino acid repeat regions exhibits both helical and β-structure propensity and makes up the proteolysis resistant core of PHFs. Here, we studied the structure and dynamics of the three-repeat domain of tau (*i.e.* K19) when bound to membranes consisting of a phosphatidylcholine and phosphatidylserine mixture or phosphatidylserine alone. Tau K19 binds to phospholipid vesicles with submicromolar affinity as measured by fluorescence spectroscopy. The interaction is driven by electrostatic forces between the positively charged protein and the phospholipid head groups. The structure of the membrane-bound state of K19 was studied using CD spectroscopy and solid-state magic-angle spinning NMR spectroscopy. To this end, the protein was selectively ^{13}C-labeled at all valine and leucine residues. Isotropic chemical shift values of tau K19 were consistent with a β-structure. In addition, motionally averaged ^{1}H–^{13}C dipolar couplings indicated a high rigidity of the protein backbone. The structure formation of K19 was also shown to depend on the charge density of the membrane. Phosphatidylserine membranes induced a gain in the α-helix structure along with an immersion of K19 into the phospholipid bilayer as indicated by a reduction of the lipid chain ^{2}H NMR order parameter. Our results provide structural insights into the membrane-bound state of tau K19 and support a potential role of phospholipid membranes in mediating the physiological and pathological functions of tau.

1. Introduction

The occurrence of fibrillar protein aggregates is a hallmark in Alzheimer's disease (AD) and related dementias [1,2]. Extracellular amyloid plaques arise from the β-amyloid peptide (Aβ) [3] and intracellular neurofibrillary tangles (NFTs) or neuropil threads are composed of regular fibrils of the microtubule-associated protein tau [4,5]. Because fibrillar lesions correlate with both neuronal cell loss [6] and cognitive decline [7] they are useful markers of neurodegeneration in AD [8]. Thus, there has been much interest in understanding the mechanisms of protein fibrillization and the cellular factors having an impact on it. In the case of the tau protein, an increase in the cytosolic concentration of unbound, hyperphosphorylated tau has been considered the pivotal event, which in its consequence can lead to protein aggregation [9,10]. However, tau has also been shown to fibrillize *in vitro* by the addition of polyanionic substances such as glycosaminoglycans (heparin, dextran sulfate) [11], polyglutamate [12], RNA [13], or by addition of fatty acids [14,15] and anionic micelles [16]. Currently, there is no genetic component known for tau aggregation in AD, but several mutations have been linked to the related neurodegenerative syndrome, frontotemporal dementia and Parkinsonism linked to chromosome 17 (FTDP-17) [17–19]. Most FTDP-17 mutations have been identified to be located near the C-terminal microtubule binding repeat regions, suggesting an important role of those regions in the formation of tau paired helical filaments (PHFs) [20]. Although tau has no *a priori* amyloidogenic

Abbreviations: Aβ, Amyloid β peptide; AD, Alzheimer's disease; CD, circular dichroism; CP, cross polarization; DIPSHIFT, dipolar coupling and chemical shift correlation; DMPC, 1,2-dimyristoyl-*sn*-glycero-3-phosphocholine; DMPS, 1,2-dimyristoyl-*sn*-glycero-3-phosphoserine; DSC, differential scanning calorimetry; FLSG, frequency-switched Lee Goldburg; FTDP-17, frontotemporal dementia and Parkinsonism linked to chromosome 17; HEPES, 2-[4-(2-hydroxyethyl)piperazin-1-yl]ethanesulfonic acid; HetCor, heteronuclear correlation; IAPP, islet amyloid polypeptide; LUV, large unilamellar vesicle; MAS, magic-angle spinning; NFTs, neurofibrillary tangles; PDSD, proton-driven spin diffusion; PHFs, paired helical filaments; POPC, 1-palmitoyl-2-oleoyl-*sn*-glycero-3-phosphocholine; POPS, 1-palmitoyl-2-oleoyl-*sn*-glycero-3-phosphoserine; SDS, sodium dodecyl sulfate; SFs, straight filaments; SUV, small unilamellar vesicle; ThT, thioflavin T; TPPM, two-pulse phase modulation

* Corresponding author. Tel.: +49 341 9715701; fax: +49 341 97 15709.
E-mail address: daniel.huster@medizin.uni-leipzig.de (D. Huster).

0005-2736/$ – see front matter © 2012 Elsevier B.V. All rights reserved.
doi:10.1016/j.bbamem.2012.03.019

sequences like *e.g.* hydrophobic regions in Aβ or polyG-sequences in the huntingtin protein (for reviews see [21,22]), short patches at the beginning of the second (^{275}VQIINK^{280}) and third (^{306}VQIVYK^{311}) repeats have been identified as aggregation motifs of tau [23]. They have been found to form the protease resistant core of PHFs by interacting as alternately stacked cross β-sheets [24–26]. In contrast, the N-terminal projection domain and proline-rich region of tau remain disordered and form a fuzzy coat surrounding the filament core [20,27]. However, apart from characterizing the structure of tau in its soluble and aggregated state, the exact mechanism of tau fibrillization and the structural transitions occurring along the aggregation process are still unknown. It is proposed that beginning from small, non-fibrillar intermediates with no observable cross β-structure and no sensitivity to thioflavin T (ThT) or congo red, tau molecules can order into either straight filaments (SFs) or more typically into paired helical filaments (PHFs) [28]. Similarly to Aβ fibrils, tau PHFs are believed to consist of protofibrils as well, however, their exact topology is still a matter of debate [29].

Soluble tau belongs to the class of natively unfolded proteins and thus has not been amenable to structure analysis by x-ray crystallography. On the other hand, nuclear magnetic resonance (NMR) spectroscopy is often hampered by a dramatic signal overlap due to the lack of ordered structure. That is why NMR studies have predominantly been performed with fragments of tau containing *e.g.* only the repeat domain (K19 or K18) [30–33]. However, the full resonance assignment and residual secondary structure determination for the longest tau isoform (441 residue tau) have been achieved recently [34]. Those experiments revealed that tau preferentially populates β-structure in the regions between repeats R2, R3 and R4 [30,31], but a weak helical [31] or much lower β-structure [30] propensity within the repeats themselves has been shown. A stable α-helix conformation in those regions was observed in the presence of anionic micelles, suggesting a structural reorganization of the protein in a membrane-like environment [33]. It is known from other amyloidogenic peptides that they often adopt a more well-ordered structure upon binding to biological membranes [35]. In that case, studies of membrane–protein interactions could also provide important mechanistic insights into the amyloidogenic pathways of the aggregation-prone peptides (for reviews see [36–38]). These findings propose a common mode, by which fibrillarized peptides and proteins could execute their cell toxic potential, *i.e.* by a perturbation of the membrane integrity [39–42]. A similar role of membranes in both tau aggregation and tau toxicity could be reasoned, too. Interestingly, tau is found attached to the neuronal cell membrane both in its non-pathologic state [43–45] and in form of PHFs in cells from AD brains [46]. Tau aggregates occur in complex with the inner cell cortex and with cell organelles already at early stages of the disease [47]. Although, free fatty acids [14,15] and anionic phospholipids [16] were shown to induce fibrillization of tau, binding to cellular membranes with multiple phospholipid components has not been analyzed yet. Furthermore, possible conformational changes of tau upon membrane binding and their role during the aggregation process have not been examined either.

Here, we report a structural study on membrane-bound tau K19. We investigated the three-repeat microtubule binding domain of tau, *i.e.* K19, in complex with phospholipid model membranes consisting of phosphatidylcholine and phosphatidylserine. Membrane–protein interactions and protein secondary structure were both studied using methods of fluorescence, CD, and solid-state NMR spectroscopy. The latter is the method of choice that can provide high resolution structural information for proteins in their complex membrane environment [48,49]. We hypothesize that the membrane-bound conformation may be important for both the normal function of tau and for its pathogenicity.

2. Materials and methods

2.1. Materials

The lipids 1-palmitoyl-2-oleoyl-*sn*-glycero-3-phosphocholine (POPC), 1-palmitoyl-2-oleoyl-*sn*-glycero-3-phosphoserine (POPS), 1,2-dimyristoyl-*sn*-glycero-3-phosphocholine (DMPC), 1,2-dimyristoyl-d_{54}-*sn*-glycero-3-phosphocholine (DMPC-d_{54}), 1,2-dimyristoyl-d_{54}-*sn*-glycero-3-phosphocholine-d_{13} (DMPC-d_{67}), 1,2-dimyristoyl-*sn*-glycero-3-phosphoserine (DMPS) and 1,2-dimyristoyl-d_{54}-*sn*-glycero-3-phosphoserine (DMPS-d_{54}) were purchased from Avanti Polar Lipids, Inc. (Alabaster, AL, USA) and were used without further purification. Sodium dodecyl-d_{25} sulfate and ^{13}C-labeled formaldehyde were purchased from Cambridge Isotope Laboratories Inc. (Andova, MA, USA). 1,2-^{13}C2-leucine and U-^{13}C5, ^{15}N-valine were purchased from Cambridge Isotope Laboratories, Inc. Further reagents and solvents were obtained from Carl Roth® GmbH (Karlsruhe, Germany) and Sigma Aldrich® Chemie GmbH (Steinheim, Germany).

2.2. Methods

2.2.1. Protein expression and purification

Recombinant protein was expressed in *Escherichia coli* cells transfected with a pET vector construct containing the DNA sequence of tau K19 under control of the T7 promoter (a kind gift from Dr. Peter Lansbury and Dr. Kenneth Kosik, Harvard Medical School). Tau K19 is a three-repeat microtubule-binding fragment, which includes the first, third, and fourth microtubule-binding repeats of tau, similarly to the naturally occurring three-repeat tau isoforms. Tau K19 consists of the residues 244–274 followed by the residues 306–372 of the sequence of the longest human tau isoform, htau40. For selective labeling, 1,2-^{13}C2-leucine and U-^{13}C5, ^{15}N-valine (both purchased from Cambridge Isotope Laboratories, Inc.) were added to ^{15}N minimal media 30 min after induction with IPTG. Purification followed the same protocol as described before [31].

2.2.2. Reductive lysine ^{13}C methylation

Reductive methylation of tau K19 was performed as described by Means and Feeney [50]. Briefly, 20 µl of 1 M borane–ammonia complex ($NH_3.BH_3$) and 40 µL of 1 M ^{13}C-formaldehyde were added to 1 mL of 0.5 mg/mL tau K19 in 200 mM CHES, pH 10.2 and the reaction was incubated for 2 h while stirring at room temperature. The addition of borane–ammonia complex and ^{13}C-formaldehyde was repeated and the mixture was incubated for another 2 h. After addition of another 10 µL of borane–ammonia complex the solution was incubated at room temperature with stirring overnight. The reaction was stopped by adding glycine to 200 mM and undesired reaction products and excess reagents were removed by dialysis against 10 mM HEPES, 10 mM NaCl, pH 7.4 in the case of solid-state NMR experiments or 10 mM Na_2HPO_4, 100 mM NaCl, pH 7.4 when using tau K19 for solution NMR.

The extent of the methylation reaction was assayed using the amino-reactive dye fluorescamine and was shown to run to completion. As analyzed by matrix-assisted laser desorption ionization (MALDI) mass spectrometry, lysine residues are mainly di-^{13}C-methylated resulting in an experimentally determined mass increase of 542 for tau K19 (as compared to a calculated increase of 544 for 17 potential free amino groups of K19).

2.2.3. Sample preparation

Large unilamellar vesicles (LUVs) of POPC/POPS or DMPC/DMPS at a molar ratio of 4:1 were formed by extrusion under nitrogen pressure through a nucleopore polycarbonate membrane [51]. Small unilamellar vesicles (SUVs) of DMPS or DMPC/DMPS were prepared by sonication as described by Huang [52]. The lipid concentration after extrusion or sonication was determined using a phosphorous assay according to the procedure of Chen et al. [53].

For NMR measurements, aliquots of LUVs were combined with isotopically labeled tau K19 dissolved in buffer A (10 mM HEPES, 10 mM NaCl, pH 7.4) to obtain a lipid:protein molar ratio of 50:1. Lipid bound tau K19 was separated from unbound protein by ultracentrifugation for 5 h at 92,500×*g* and 4 °C. The pellet was frozen in liquid nitrogen and lyophilized under a vacuum of ~0.1 mbar over night. Subsequently, the sample was rehydrated to 50 wt.% by adding water and equilibrated by freeze-thaw cycles, stirring and gentle centrifugation. Finally, the sample was transferred to a 4 mm MAS rotor equipped with a cylindrical Teflon insert providing a volume of 50 μL.

For static ^{2}H and ^{31}P NMR measurements, unlabeled tau K19 was used. The samples were prepared in analogy to the NMR samples with isotopically labeled tau K19.

2.2.4. Fluorescence measurements

The intrinsic fluorescence of tau K19 was measured with an ISA Jobin Yvon SPEX FluoroMax-2 spectrofluorometer (Jobin-Yvon, Edison, NJ, USA). An excitation wavelength for tyrosine of 278 nm was used. Spectra were recorded in the region of 290–410 nm and were averaged to achieve an adequate signal to noise ratio. After background correction, the spectra were fitted to a log-normal distribution [54]:

$$I(\lambda) = I_{\max} \exp\left[-\frac{\ln 2}{\ln^2 \rho} \ln^2\left(1 + \frac{(\lambda-\lambda_{\max})\left(\rho^2-1\right)}{\rho\Gamma}\right)\right], \quad (1)$$

where I_{max} is the intensity observed at the wavelength of maximum intensity λ_{max} and Γ is the full width of the spectrum at half-maximum intensity $I_{max}/2$. The asymmetry of the distribution is described by the parameter ρ. Nonlinear least-squares fitting was performed with Origin 6.0 (MicroCal. Inc., Northhampton, MA, USA) to determine the intensity at constant wavelength, which was obtained for I_{max} in the spectrum of complete membrane-bound tau K19 (~303 nm). The fraction of membrane-bound protein was calculated according to Ladokhin et al. [54]:

$$f_b = \frac{I-I_0}{I_\infty - I_0}, \quad (2)$$

where f_b denotes the membrane-bound fraction, I_0 is the fluorescence intensity in the absence of lipid and I_∞ is the fluorescence intensity that corresponds to complete binding. Intensity values were fitted to a one-site model [54]:

$$I([L]) = I_0 + (I_\infty - I_0)\left(\frac{k[L]}{[W] + k[L]}\right), \quad (3)$$

with [*L*] the lipid concentration, *k* the mole-fraction (X) partition coefficient ($k = X_{bilayer}/X_{water}$) and [*W*] the molar concentration of water (55.5 M). The respective K_D value for the transfer between the membrane and water was determined from the mole-fraction partition coefficient ($K_D = [W]/k$) [55].

2.2.5. Leakage assay

Liposomes for the leakage assay were prepared as described under Section 2.2.3. Buffer A contained additionally 60 mM of 6-carboxyfluorescein. At this concentration, carboxyfluorescein is self-quenched. The external fluorophor was removed from the sample by eluating 500 μL of the liposome solution trough a Sephadex G-50 column (GE Healthcare, Munich, Germany) with isotonic buffer solution. The leakage experiments were performed on a FluoroMax-2 spectrofluorometer (Jobin-Yvon, Edison, NJ, USA) at 25 °C. The excitation wavelength was set at 485 nm and the fluorescence signal was detected at 515 nm. About 20 μL of the eluated liposomes was diluted in 2.5 mL of isotonic buffer solution. The leakage of the liposomes after adding the protein dilutes carboxyfluorescein below 10 mM and diminishes the fluorophor self-quenching. The leakage extent was calculated by $(I-I_0)/(I_T-I_0)$, where I_0 was the fluorescence intensity before adding the protein, *I* the observed fluorescence signal and I_T the fluorescence intensity after adding 2% (v/v) of Triton X-100.

2.2.6. Thioflavin T (ThT) assay

The formation of tau filaments was assayed using ThT fluorescence, which is sensitive to amyloid deposits [56]. To this end, 6 μM of tau K19 was added to 60 μM freshly filtered ThT in buffer A and incubated together with 600 μM of POPC/POPS or DMPC/DMPS LUVs for several days at 37 °C and under continuous shaking. In this assay, the presence of tau filaments is expected to result in a greatly increased ThT fluorescence at ~480 nm. The excitation wavelength was set to 450 nm and spectra were recorded in the region of 460–520 nm. Control spectra were collected in the absence of protein and in the presence of aggregated tau K19.

2.2.7. Circular dichroism (CD) spectroscopy

CD measurements were carried out on a Jasco J-715 CD spectrophotometer. Tau K19 was prepared at different mixing ratios with SUVs of DMPC/DMPS (mol% 80:20), DMPS, or with SDS in buffer B (10 mM Na_2HPO_4, 10 mM NaCl, pH 7.4) and incubated for 30 min prior to measurements. The protein concentration was 5 μM. CD spectra were acquired in the region of 190–250 nm with a scan rate of 50 nm min^{-1}, an increment of 1 nm and a response time of 1 s. Ten spectra were averaged and background corrected (using the CD spectra of buffer B or buffer B with SUVs). The secondary structure content (α-helix, β-sheet, turn and random coil) was estimated using three different deconvolution algorithms (CONTIN [57], CDSSTR [58], and SELCON [59]) with reference dataset 7 from the DICROWEB website.

2.2.8. DSC measurements

DSC measurements were performed with a Nano Differential Scanning Calorimeter (TA Instruments, Lindon, UT). All samples were degassed for at least 20 min prior injection and were heated from 5 °C to 50 °C with a scan rate of 1 K/min relative to Buffer B containing equal amounts of tau K19. DSC curves were baseline corrected and the main phase transition enthalpy and temperature were determined using the supplied software NanoAnalyze™ 2.0 (TA Instruments, Lindon, UT).

2.2.9. Static solid-state NMR experiments

^{31}P NMR experiments were carried out on a Bruker DRX300 spectrometer (Bruker BioSpin, Rheinstetten, Germany) operating at a resonance frequency of 121.3 MHz for ^{31}P using a 5 mm double resonance probe. ^{31}P NMR spectra were acquired using a Hahn echo pulse sequence with a delay between pulses of 60 μs, a typical 90° pulse length of 1.05–1.15 μs, a spectral width of 100 kHz and a recycle delay of 2 s. Broadband ^{1}H decoupling was applied during signal acquisition. The temperature was 37 °C for all samples. To determine the chemical shift anisotropy (Δσ), ^{31}P spectra were simulated for different Δσ values using Mathcad (Mathsoft, Inc., Cambridge, MA). Due to the spherical distribution of the lipid molecules, powder averaging was performed in 1° increments for the β Euler angle.

^{2}H NMR spectra were recorded on a Bruker Avance 750 MHz spectrometer at a resonance frequency of 115.3 MHz for ^{2}H using a probe with a 5 mm solenoid coil. ^{2}H NMR spectra were accumulated using a quadrupolar echo sequence with a 90° pulse length of 2.3–2.65 μs, a delay between pulses of 60 μs and a recycle delay of 0.5 s. The temperature was 37 °C for DMPC/DMPS (80:20 mol%) and 53 °C for DMPS, respectively. ^{2}H NMR spectra were dePaked using the

method of McCabe and Wassall [60] and order parameter for each methylene group was calculated according to references [61,62].

2.2.10. Solution NMR experiments

Standard ^{1}H–^{13}C HSQC experiments with double inept transfer and phase selection through echo/antiecho-TPPI gradient selection [63] were recorded on a Bruker DRX600 spectrometer (Bruker, Rheinstetten, Germany) using a 5 mm triple-inverse probe at 25 °C. For each increment 24 scans were recorded with spectral widths of 6 kHz for ^{1}H and 6 kHz for ^{13}C as well as 128 data points in the ^{13}C dimension.

2.2.11. MAS NMR experiments

MAS NMR experiments were carried out on a Bruker Avance 750 MHz spectrometer at resonance frequencies of 749.9 MHz for ^{1}H and 188.6 MHz for ^{13}C. A double resonance probe equipped with a 4 mm spinning module was used. Experiments were carried out at 37 °C for DMPC/DMPS and 53 °C for DMPS.

^{13}C CP MAS spectra were acquired using a 4 μs long ^{1}H 90° excitation pulse and a cross-polarization (CP) contact time of 700 μs. The radio frequency field strength for heteronuclear two-pulse phase modulation (TPPM) decoupling [64] was 62.5 MHz. Typical 90° pulse lengths used in the following experiments were 4 μs for ^{1}H and 6 μs for ^{13}C. The MAS frequency of all samples was 7 kHz. Chemical shifts were referenced with respect to the ^{13}CO signal of ^{13}C-labeled glycine at 176.45 ppm (relative to TMS) that was used as external standard. Two-dimensional (2D) ^{13}C–^{13}C correlation spectra were obtained using a proton-driven spin diffusion (PDSD) experiment [65]. Spin diffusion periods of 100 and 500 ms were applied.

Two-dimensional ^{1}H–^{13}C heteronuclear correlation (HetCor) spectra [66] were measured using the same parameters as for ^{13}C CP MAS spectra. ^{1}H chemical shifts were referenced to the DMPC-glycerine-G2 protons at 5.31 ppm relative to TMS [67].

The strength of the ^{13}C–^{1}H dipolar coupling was measured using the constant time dipolar coupling and chemical shift (DIPSHIFT) experiment [68]. ^{1}H–^{1}H homonuclear decoupling was achieved using the frequency-switched Lee–Goldburg (FSLG) sequence [69]. The 360° ^{1}H pulses had a duration of 15.3 μs, yielding an effective decoupling field strength of 80 kHz. The MAS frequency was 7 kHz. The signal was only acquired over one rotor period since the signal decay induced by dipolar coupling is periodic with the rotor period. The resulting spectra were only Fourier transformed in the direct dimension and the dipolar dephased signal for each resolved peak was extracted and simulated with Mathcad to obtain the dipolar coupling. Simulations were performed for varying dipolar coupling strengths with powder averaging in 2° increments for the β and γ Euler angles. Other input parameters included the number of t_1 increments, the dwell time and the spinning rate.

The molecular order parameters for the C–H bonds (S_{CH}) were calculated by dividing the measured dipolar coupling by rigid limit values, which were obtained from measurements of crystalline amino acids as reference for full dipolar coupling: CH (Ala, 13.7 kHz), CH_2 (Gly, 16.3 kHz) and CH_3 (Ala, 22.8 kHz) [70].

3. Results

3.1. Membrane interaction of Tau K19

The interaction of tau K19 with membranes was first probed using liposomes composed of PC and PS at a molar ratio of 4:1, since membranes from AD brains have been shown to contain significantly higher levels of PS [71,72]. Fig. **1** shows the binding of tau K19 to DMPC/DMPS vesicles that was detected by a change in the intrinsic tyrosine fluorescence of the protein when partitioning into the lipid bilayer. The K_D value was determined by fitting the fluorescence intensities to a one-site binding model. In general, tau K19 shows a high affinity for phospholipid membranes yielding a K_D of (53.3 ± 18.3) μM for POPC, which corresponds to a protein:lipid ratio of approximately 1:7. Not surprisingly, the binding is even stronger for a membrane containing 20 mol% of negatively charged PA or PS and reaches its maximum for pure DMPS (Table 1). The nature of the phospholipid acyl chain has no observable effect on the K_D value. Furthermore, the binding affinity also depends on the ionic strength as demonstrated by a decrease of the K_D at 10 mM NaCl compared to 100 mM. These data suggest that the interaction of tau K19 with the lipid bilayer is mostly driven by electrostatic forces between the phospholipid headgroups and the protein, which has a high positive charge under physiological conditions (net charge of +7.1).

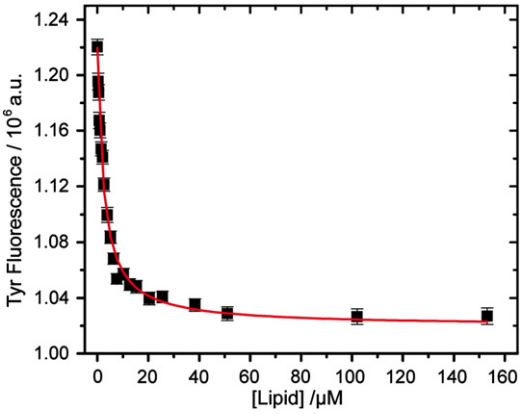

Fig. 1. Change in the tyrosine fluorescence intensity of 8 μM tau K19 as a function of the titrated liposome concentration. Liposomes consisted of DMPC/DMPS (80/20 mol/mol) in buffer A (10 mM HEPES, 100 mM NaCl, pH 7.4) at 25 °C. Error bars for each titration point were obtained from the fit of the fluorescence spectrum to a log-normal distribution by the Levenberg–Marquel algorithm, which is implemented in the Origin 6.0 software. The fluorescence intensities were fitted to a one site binding model. Dissociation constants (K_D) are given in Table 1.

Further evidence for a membrane binding of K19 was provided from DSC measurements using DMPC/DMPS vesicles. As expected from the larger surface area of the PS headgroup compared to PC, the enthalpy of the main phase transition is increased with higher DMPS content in the absence of tau K19. However, upon adding tau K19 the phase transition gets broadened, especially for DMPS contents of 40 and 80% (Supplementary Fig. 1), and the transition enthalpy is decreased in a concentration dependent manner *i.e.* it is the lowest for pure DMPS (Fig. **2**). This observation suggests a preferential interaction of tau K19 with the negatively charged PS molecules. Despite broadening of the phase transition we could not find a clear evidence for a lipid demixing of the membrane *e.g.* by an asymmetry of the DSC traces. Only for a PC/PS ratio of 4/1 the occurrence of the $L_{\beta'}$–$P_{\beta'}$ prephase transition of DMPC is observed, which would argue for a partial demixing by tau K19 in that case.

Table 1
K_D values for the titration of tau K19 with phospholipid vesicles depending on the content of negatively charged phosphatidate (PA) or phosphatidylserine (PS) and on the sodium concentration. The temperature was 25 °C except for DMPS, which was measured at 37 °C.

Lipid composition (mol%)		NaCl (mM)	K_D ± S.D. (μM)
POPC	100	100	53.3 ± 18.3
DMPS	100	100	0.22 ± 0.04
POPC/POPA	80:20	100	7.97 ± 4.34
POPC/POPS	80:20	100	0.93 ± 0.08
DMPC/DMPS	80:20	100	2.40 ± 0.18
POPC/POPS	80:20	10	0.42 ± 0.06
DMPC/DMPS	80:20	10	0.38 ± 0.10

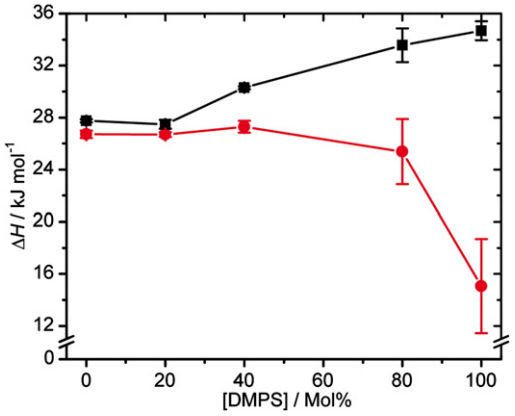

Fig. 2. Enthalpy of the main phase transition of DMPC/DMPS LUVs with increasing content of DMPS both in the absence (■) and in the presence of 2 mol% tau K19 (●). The DSC curves were recorded in buffer A. Error bars represent standard deviations of three independent measurements.

However, the prephase transition was not detected when the DMPS content was further increased.

The previous results are consistent with the detected ^{31}P NMR spectra of DMPC/DMPS vesicles (Supplementary Fig. 2). The spectra show a typical powder line shape confirming the liquid crystalline lamellar bilayer structure of the membrane. The shoulder of the peak at lower field indicates a superposition of the spectra of both phospholipids in the sample. By simulating the spectral line shapes $\Delta\sigma$ values of 44.4 ppm and 54.3 ppm were obtained and assigned to DMPC and DMPS, respectively. In the presence of 2 mol% tau K19, the $\Delta\sigma$ value of DMPC is reduced by 2.8 ppm and that of DMPS by even 4.0 ppm indicating a conformational perturbation of the phospholipid headgroups induced by the protein. This effect is again more significant for DMPS than for DMPC.

In contrast to the phospholipid headgroups, only a negligible influence of tau K19 on the lipid chain conformation is found in ^{2}H NMR experiments. In the presence of the protein, the average order parameter of the lipid chain is slightly increased from 0.160 to 0.163 for DMPC-d_{54} and from 0.173 to 0.177 for DMPS-d_{54} (Fig. 3a), indicating that there is essentially no penetration of the protein into the hydrophobic core of a DMPC/DMPS membrane. However, using vesicles consisting of only DMPS, tau K19 clearly induces a very dramatic decrease in the lipid chain conformational order (Fig. 3b), which can be explained by an insertion of the protein into the acyl chain region of the bilayer. The average order parameter for the entire lipid chain is decreased from 0.231 in pure DMPS-d_{54} membranes to 0.159 in the presence of tau K19. This loss of order leads to a reduction of the molecular packing density and an increase in the area per DMPS molecule in the membrane, which can be quantified according to Ref. [73]. Thus, an increase in area per molecule of 6.5 Å^2 as a consequence of tau K19 binding was calculated.

Since it is demonstrated that tau K19 can penetrate into the lipid bilayer, the question arises if that behavior can lead to a disruption of the membrane integrity. Thus, we performed vesicle leakage experiments for both DMPC/DMPS and DMPS alone. Interestingly, tau causes a tremendous leakage of DMPS vesicles, which are disrupted to ca. 95% by 5 mol% of the protein within 2 min (Supplementary Fig. 3). In comparison, DMPC/DMPS vesicles show a smaller content of leakage but 4 mol% of tau K19 still lead to 15% leakage within 12 min (Supplementary Fig. 3). It is obvious that the membrane disruption occurs very fast and is completed already after a few minutes. That observation would argue for a membrane pore formation. In contrast, a bilayer disruption caused by a detergent-like mechanism of the protein would follow a slower, constantly increasing kinetics.

When searching for possible lipid binding sites within tau K19, it is reasonable that the positively charged side chains of basic amino acids can directly interact with the negatively charged phospholipid headgroups. Interestingly, lysine is the most frequent amino acid residue in K19. In order to detect such binding events in NMR experiments, the lysine ε-amino groups were ^{13}C-methylated by reductive alkylation [50]. Due to the natively unfolded structure of tau K19 in solution, the lysine side chains are probably well surface exposed. Thus, the labeling reaction went to completion as assayed with the amino group sensitive dye fluorescamine and by mass spectrometry.

Binding contacts with the membrane, *e.g.* salt bridges, will change the electronic environment of the ^{13}C nuclei in the amino attached methyl groups, which will consequently lead to changes in their chemical shifts. Fig. 4 shows the ^{1}H–^{13}C HetCor spectra of ^{13}C-methylated tau K19 in the presence of DMPC and DMPC/DMPS vesicles acquired under magic-angle spinning (MAS) conditions. For comparison, standard ^{1}H–^{13}C HSQC spectra of tau K19 in solution and after addition of 150 mM SDS are superimposed. Most of the ^{13}C-methyl groups cluster at one major peak at a ^{1}H chemical shift of 2.85 ppm and a ^{13}C chemical shift of 39.5 ppm. However, there are also $^{13}CH_3$ signals at lower and higher field, displaced up to 0.8–1.4 ppm in the ^{1}H dimension and by 1.2 ppm in the ^{13}C

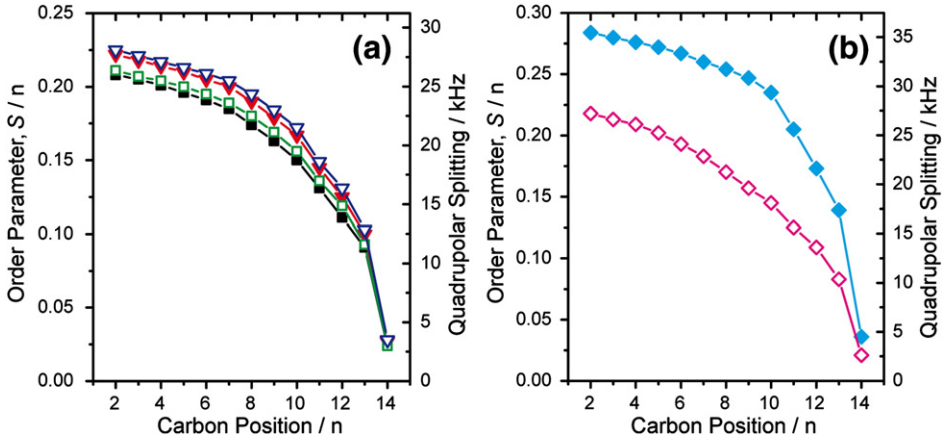

Fig. 3. Smoothed ^{2}H NMR order parameter profiles of the lipid methylene groups in DMPC/DMPS (a) and DMPS LUVs (b) in the absence and in the presence of 2 mol% tau K19 in 50 wt.% of buffer A (10 mM HEPES, 10 mM NaCl, pH 7.4). The temperature was 37 °C for DMPC/DMPS and 53 °C for DMPS. In (a) the curves represent the order parameter profile for DMPC-d_{54} with (□) and without (■) tau K19 and for DMPS-d_{54} in the presence (▽) and in the absence (▼) of the protein. Symbols in (b) are DMPS-d_{54} without (◆) and with tau K19 (◇).

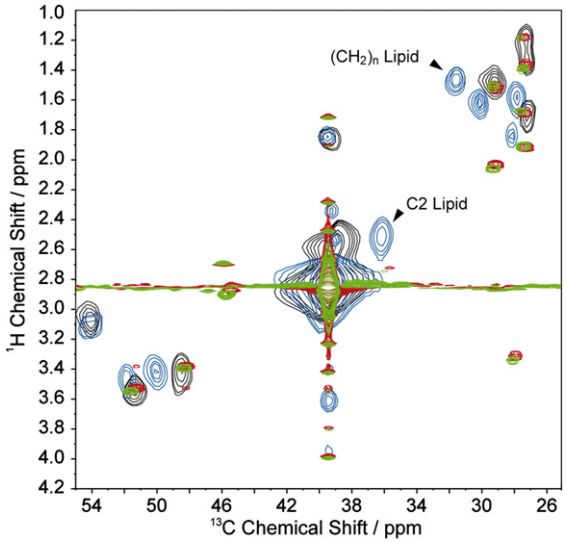

Fig. 4. Contour plot of $^{1}H–^{13}C$ heteronuclear correlation (HetCor) spectra of 2 mol% lysine N^{ε} ^{13}C-methylated tau K19 in complex with DMPC (black) and DMPC/DMPS (blue) vesicles measured at 37 °C with a MAS spinning rate of 7 kHz. For comparison, the HSQC NMR spectrum of free ^{13}C-methylated tau K19 in solution (red) and in the presence of 150 mM SDS (green) is indicated.

dimension. For DMPC, the peaks overlap closely with those of soluble tau indicating no considerable interactions of the lysine residues of tau K19 with the DMPC membrane. However, the fact that a moderate binding is also observed for the uncharged POPC (see Table 1), suggests that other energetic effects contribute to tau K19 membrane binding in addition to electrostatics. In the presence of SDS, the $^{13}CH_3$ signals are slightly downfield shifted, which argues in favor of an interaction of the lysine side chains with the micelles. When DMPC/DMPS membranes are used, the position of the corresponding $^{13}CH_3$ correlations is even more altered. This observation further confirms the involvement of lysine in the membrane binding of tau K19. A different binding mode of the protein in its conformationally more complex membrane environment as compared to SDS micelles, may further explain the even more pronounced chemical shift alterations of the $^{13}CH_3$ signals in the DMPC/DMPS membrane.

3.2. Conformation of Tau K19 in a membrane environment

Using far-UV CD spectroscopy the effect of DMPC/DMPS and DMPS vesicles on the overall conformation of tau K19 was analyzed (Fig. 5). As reported previously [33], tau K19 undergoes remarkable conformational changes in the presence of SDS micelles and lipid vesicles. When free in solution, K19 is essentially unstructured, but in the presence of DMPS and SDS the protein adopts significant α-helical structure as indicated by a lineshape change of the CD spectra and a decrease of the ellipticity at 208 and 222 nm. This structural change is shown to be concentration dependent and a deconvolution of the CD spectra using the DICROWEB database reveals the highest α-helix content for 2 mM DMPS (approximately 22%). However, a considerable content of β-sheet structure of 25–28% is also predicted from data deconvolution. It has to be mentioned here that deconvolution of the CD data was difficult due to noise below 190 nm, which is mostly caused by light scattering at the lipid vesicles. That is why we are careful with estimating the exact content of secondary structure. In comparison to SDS and DMPS, the observed conformational change is much lower for mixed DMPC/DMPS vesicles (mol% 80:20). The lineshape of the CD spectra is only slightly changed compared to free tau K19 and the signals at 208 and 220 nm are much weaker than for negative DMPS indicating no reasonable α-helical content. Since tau K19 was shown to bind DMPC/DMPS and DMPS vesicles with the same high affinity (Table 1) it is unlikely that this observation results from an equilibrium of vesicle bound and free tau K19. Rather, it is more likely that this represents a different protein conformation at membranes with lower surface charge. Interestingly, deconvolution of the CD spectra again reveals a partial β-structure content.

To further investigate the secondary structure of tau K19 in the membrane environment at residue resolution, isotropic chemical shifts for a selectively labeled tau K19 (with ^{13}C labeled valine and leucine residues) were determined by ^{13}C solid-state MAS NMR spectroscopy. Isotropic chemical shifts are empirically correlated to protein secondary structure *e.g.* a downfield shift of the ^{13}C Cα and CO signals compared to the random coil values and a simultaneous upfield shift of the Cβ signal indicate a helical structure. The opposite chemical shift changes are correlated to β-sheet structures [74–76]. The isotropic ^{13}C chemical shifts for the valine and leucine residues in tau K19 were assigned from two-dimensional $^{13}C–^{13}C$ correlation spectra (Fig. 6) recorded by proton driven spin diffusion (PDSD) experiments and are summarized in Table 2. A spin diffusion time of 100 ms was used, which allows magnetization to transfer between two ^{13}C spin pairs separated by up to three bonds. Thus, cross peaks occur only within a labeled amino acid and allow the assignment of all protein signals.

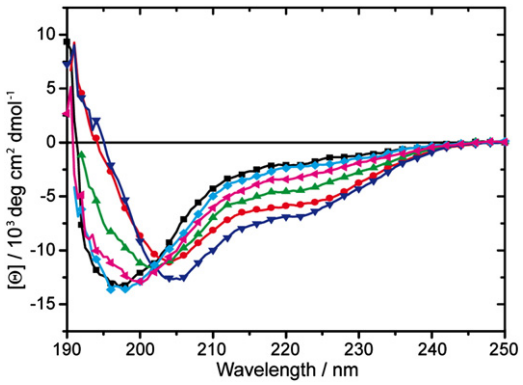

Fig. 5. Far UV CD spectra of tau K19 in buffer B (10 mM Na_2HPO_4, 10 mM NaCl, pH 7.4) at 37 °C. The spectra represent free tau K19 (■) and tau in the presence of 5 mM SDS (●), 0.5 mM (◆) and 2 mM (◀) DMPC/DMPS or 0.5 mM (▲) and 2 mM (▼) DMPS.

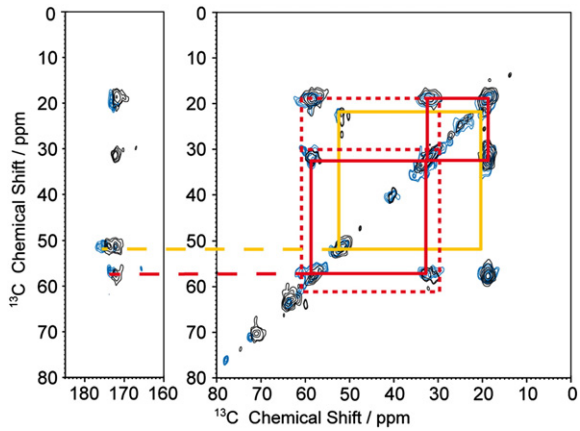

Fig. 6. Contour plot of $^{13}C–^{13}C$ correlation spectra of 2 mol% tau K19 in DMPC/DMPS (black) and DMPS (blue) vesicles at a MAS spinning rate of 7 kHz. $^{13}C–^{13}C$ correlations were established by a proton driven spin diffusion period of 100 ms. Nearest neighbor correlations for valine (red) and leucine (yellow) are indicated. Chemical shift values and signal assignments are given in Table 2.

Table 2
Isotropic ^{13}C chemical shift values of tau K19 in DMPC/DMPS or DMPS membranes and corresponding protein secondary structure determined from ^{13}C–^{13}C correlation spectra. ^{1}H–^{13}C dipolar couplings ($\bar{\delta}$) and CH order parameters (S_{CH}) were measured with the DIPSHIFT experiment.

			Chemical shift (ppm)		Difference Cα–Cβ (ppm)	Secondary structure	$\bar{\delta}$ (kHz)	S_{CH}
			Experiment	Reference*				
DMPC/DMPS	Val	$^{13}C\alpha$	58.4	58.0[b]	26.3 (25.6[b])	Sheet	11.6	0.85
		$^{13}C\beta$	32.1	32.4[b]			10.3	0.75
		^{13}CO	172.2	172.4[b]			–	–
	Leu	$^{13}C\alpha$	51.8	51.7[b]	–	Sheet	12.2	0.89
		^{13}CO	173.8	173.1[b]			–	–
DMPS	Val	$^{13}C\alpha$	61.6	63.0[a]	31.4 (33.1[a])	Helix	8.6	0.63
		$^{13}C\beta$	30.2	29.9[a]			–[d]	–[d]
		$^{13}C\alpha$	58.7	58.0[b]	26.6 (25.6[b])	Sheet	12.3	0.90
		$^{13}C\beta$	32.1	32.4[b]			11.9	0.87
		^{13}CO	173.4	173.1[c]		Coil	–	–
	Leu	$^{13}C\alpha$	53.1	52.5[c]	–	Coil	9.7	0.71
		^{13}CO	175.2	176.3[a] (174.4[c])		Helix/Coil	–	–

*Reference values are empirical data for α-helix[a], β-sheet[b] and random coil[c] conformation [104]. All chemical shifts are relative to TMS. [d]Signal on noise level.

To check if long range correlations are present in tau K19/membrane samples, PDSD experiments with mixing times of 500 ms were also performed. Correlations of longer distance could result from intramolecular folding or from intermolecular aggregation of the protein. However, no additional cross peaks were observed at a mixing time of 500 ms.

In complex with DMPC/DMPS (mol% 80:20) membranes, the chemical shifts of the individual valine and leucine carbons in all labeled residues of tau K19 are nearly identical, *i.e.*, no individual residues could be identified. In each case, their peaks overlap and no additional population for valine and leucine with a different conformation could be observed. Furthermore, the chemical shifts are nearly identical for two measured protein:lipid ratios of 1:50 and 1:250.

In comparison to tau K19 free in solution and in the presence of micelles, the Cα signals of valine and leucine are upfield shifted when bound to membrane vesicles. Besides, all backbone carbon atoms *i.e.* carbonyl groups and Cα atoms exhibit an upfield shift relative to empirical reference values for random coil conformation. Simultaneously, the Cβ side chain signal of valine is displaced to lower field. Hence, all ^{13}C chemical shifts are indicative for a β-sheet structure of tau K19 in its membrane environment. This contrasts the results from solution NMR of tau K19 in the presence of micelles [33], where the valine and leucine signals show clear chemical shifts that are in agreement with an α-helix structure (Fig. 7).

Since referencing of chemical shifts in solid-state NMR remains challenging due to the lack of an appropriate internal standard, we also analyzed the Cα–Cβ differences, which are independent of external referencing. Thus, errors resulting from absolute chemical shift determination can be avoided. In DMPC/DMPS membranes, the Cα–Cβ difference for valine is 26.3 ppm, which is in good agreement with the reference value for β-sheet structures of 25.6 ppm.

Additional information on the protein secondary structure could be obtained from the analysis of the protein backbone and side chain dynamics. To this end, dipolar couplings of the C–H bond vectors were determined by the two-dimensional DIPSHIFT experiment. Since dipolar couplings are partially motional averaged, they provide order parameters of the amplitude of motion at the respective protein site. Quantitative values of the dipolar coupling strength are listed in Table 2 and were converted to molecular order parameters as specified under Materials and methods. For both labeled amino acid residues high order parameters of the Cα position were determined indicating a high rigidity of the protein backbone of tau K19. In addition, also the first side chain position of valine shows a high degree of order compared to other membrane-bound peptides with β-sheet structure [70,77].

Changing the DMPC/DMPS membrane to pure DMPS vesicles has minor effects on the Cα and Cβ chemical shifts of valine. However, the CO signal is displaced to lower field by 1.2 ppm indicating that at least some of the valine residues in tau K19 undergo a conformational change at the protein backbone. The chemical shift was found to be 173.4 ppm, which is consistent to a random coil conformation with an empirical reference value of 173.1 ppm. Furthermore, an additional shoulder of the valine Cα cross peaks is detected in the ^{13}C–^{13}C correlation spectrum. These correlations are found at 61.6 ppm and 30.2 ppm, which is close to reference values of α-helical conformation at 63.0 ppm and 29.9 ppm. However, for most

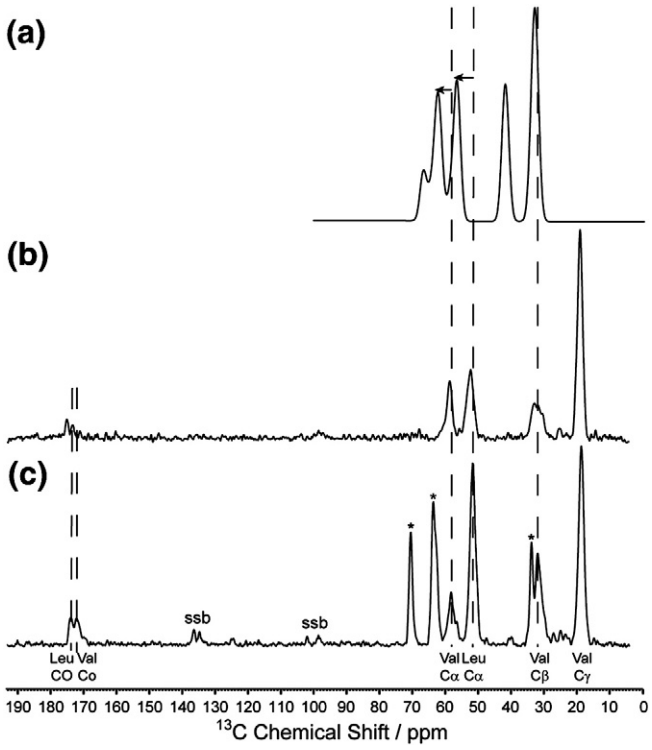

Fig. 7. Proton-decoupled 188.6 MHz ^{13}C CP MAS spectra of 2 mol% tau K19 in (b) DMPS vesicles and (c) DMPC/DMPS membranes at a buffer content of 50 wt.% and a temperature of 53 °C or 37 °C, respectively. The MAS spinning rate was 7 kHz. For comparison a one dimensional spectrum for the Cα and Cβ signals of valine and leucine based on the ^{13}C chemical shifts of tau K19 in SDS micelles [33] is simulated in (a). A downfield shift of the Cα peak for both amino acids compared to the signals in DMPC/DMPS membranes is indicated by arrows. Lipid signals are marked with an asterisk and ssb denotes spinning sidebands.

valine residues tau K19 maintains a β-structure, which can be concluded from the intensity ratio of the corresponding cross peaks. In contrast, the Cα and CO signals of leucine are clearly upfield shifted in comparison to tau K19 in DMPC/DMPS membranes. The differences are 1.3 ppm and 1.4 ppm, respectively. The Cα chemical shift (53.1 ppm) indicates a random coil whereas the CO signal of leucine (175.2 ppm) can be classified to either α-helix or random coil, respectively. These results suggest a structural change of tau K19 in DMPS membranes and are in agreement with the partial α-helical structure of K19 in the presence of negatively charged micelles [33]. They may also reflect the observed differences in the mode of interaction for two different membrane environments. Although there are 10 labeled valine and only 6 labeled leucine residues in tau K19, the observed conformational changes are more clearly detectable for the leucine sites, whereas most valine residues retain their β-structure. This observation suggests that restricted regions within the protein may undergo a structural transformation for instance three short patches in the center of each pseudo repeat region, which were reported by Barré et al. [33]. In contrast, other regions *e.g.* the aggregation motif PHF6 at the beginning of repeat R3 could maintain a β-structure. Noteworthy, this 9 amino acid long sequence contains three valine residues.

In addition to isotropic chemical shifts, also dynamic information obtained from dipolar couplings of the C–H bond vector suggests a change of the protein secondary structure in DMPS membranes. The order parameter of the leucine Cα atom is significantly reduced to 0.71, which indicates a higher flexibility at the protein backbone and is consistent with a gain of α-helix structure. In contrast, the valine residues retain a high rigidity at the Cα and Cβ positions with order parameters of 0.90 and 0.87, which makes their location in regions of β-structure very likely.

Since tau K19 is known to form PHFs, which exhibit significant β-structure, the aggregation potential of K19 in the presence of lipid vesicles was tested using ThT fluorescence. Tau filaments lead to a large increase of the ThT fluorescence at ~480 nm when excited at 450 nm, which was confirmed by heparin-induced self-assembly of tau (Supplementary Fig. 4). However, POPC/POPS and DMPC/DMPS vesicles did not increase the ThT fluorescence over the observed time course of several days up to one week. This corresponds to the duration of some of the NMR experiments. Thus, a filament formation of membrane-bound tau K19 could not be detected here. Rather, it is possible that a different type of β-structure is formed by tau K19 in its membrane environment, for instance smaller monomeric or oligomeric structures, which are insensitive for ThT. They could also assemble to a pore-like structure that would explain the membrane disruption potency of tau observed in the leakage experiments.

4. Discussion

Understanding the pathogenic mechanisms, which lead to a transformation of the natively unstructured protein tau into highly ordered protein fibrils is pivotal for an elucidation of its cell toxic potential in neurodegenerative tauopathies *e.g.* Alzheimer's disease. During the last decades, the contribution of several factors *e.g.* genetic mutations [17–19], posttranslational modifications [78], oxidative stress [79,80] and poly-anionic substances [11–13] in the tau fibrillization pathway has been investigated. As for other amyloidogenic proteins, biological membranes have been suggested to be relevant for the aggregation of tau as well [33]. The presence of anionic detergents or lipids has been shown to greatly enhance tau fibril formation, suggesting the structure of the protein in complex with cellular membranes to be relevant for tau aggregation and toxicity [16]. Moreover, early tau aggregates bearing already a decisive β-structure as well as mature tau PHFs have been both found to be attached to cellular membranes and organelles [47,81].

Several mechanisms could be imagined, by which lipid membranes act as a template for protein misfolding and subsequent ordering into fibrils [38]. Membrane binding increases the local protein concentration and reduces the dimensionality from three dimensions in solution to two at the membrane surface. Thereby, the conformational entropy could be reduced, which imparts structural ordering and leads to secondary structure formation [35]. In that respect, biological membranes also provide a special physicochemical microenvironment that can influence *e.g.* the protonation state of protein residues, which may also affect secondary structure formation. Furthermore, the local solvent dielectric constant is lowered on the membrane surface, which may facilitate the formation of intermolecular hydrogen bonds in β-sheet aggregates.

In addition, to the role of membrane binding in tau pathology, interactions with the lipid bilayer could also be relevant for the normal function of tau. Tau was shown to bind to the neuronal cell membrane when expressed in PC12 cells [43,45] and it was hypothesized that one of tau's functions may involve attaching microtubules to membranes.

Here, we report that the three repeat domain of tau, K19, adopts a significant β-structure upon binding to membrane vesicles composed of DMPC and DMPS at a molar ratio of 4:1. The chemical shifts of the measured valine and leucine residues are consistent with reference values for those amino acids in β-sheets. In addition, the order parameters indicate a high rigidity of the protein backbone and of the first side chain position, which is typical for amino acids in ordered fibrillar β-strands [82]. The ^{13}C-labeled valine and leucine residues are located mainly in the first half of each repeat region especially in the case of repeat R3 (Fig. **8**). The sequence ^{306}VQIVYKPV^{313} for instance comprises three valine residues and contains the so-called PHF6 aggregation motif [23]. This motif has been shown to adopt a strand-like conformation in the free state of tau [30,34] and makes up the protease resistant core of PHFs [25,26]. It is known to play a key role in nucleating tau filament formation. Furthermore, the successive sequence motif ^{314}DLSKVTSK^{320} was also shown to be crucial for tau fibrillization [83] and exists in a β-structure in the core of PHFs as well [26]. Finally, also the region ^{337}VEVKSEKLD^{345} at the beginning of repeat R4 exhibits a strand-like conformation in the free state of tau [30,31]. Hence, β-structure elements in membrane-bound tau

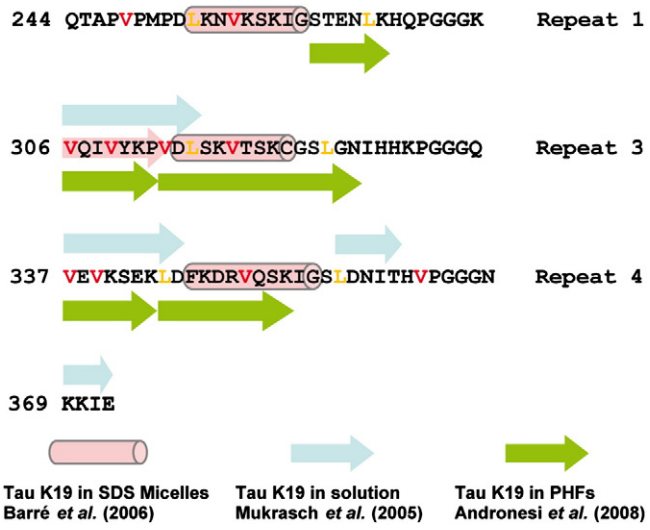

Fig. 8. Comparison of type and location of secondary structure elements of tau K19 in three different states: micelle-bound [33] (pink), free in solution [30] (blue) and in PHFs [26] (green). The ^{13}C-labeled residues, which were detected in this study, are marked red for valine and yellow for leucine. Helices are indicated by cylinders and β-strands are simplified by arrows.

K19 are likely to show a similar topology as in the solution state of tau K19. Also, an elongation of the strand regions in a similar way as in the core structure of K19 PHFs [26] is possible. Interestingly, based on the isotropic chemical shifts we found no evidence for an α-helix structure of tau K19 upon binding to DMPC/DMPS membranes. In contrast, a different lipid environment, *i.e.* anionic DMPS vesicles, induces a conformational change of the protein towards random coil and partially α-helix, which is more pronounced for leucine and less significant for valine. That structure of tau K19 in complex with anionic phospholipids could resemble the micelle-bound state of the protein [33] comprising three helical patches within the center of each pseudo repeat region. It is possible that the chemical shift changes are more important for leucine since these residues may be located within the helix regions whereas the valine residues reside in regions of β-structure *e.g.* the PHF6 aggregation motif in repeat R3 or the ^{337}VEVKSEKLD^{345} sequence at the beginning of R4 (Fig. **8**). Furthermore, it is known that Cβ-branched amino acids like threonine, valine, or isoleucine have an intrinsic preference to be located in β-strands in the middle of β-sheets [84,85], even though β-structure formation is determined also in large part by tertiary contacts.

Based on the available structural data a two-state model for the interaction of tau K19 with phospholipid membranes can be proposed (Fig. **9**). In mixed DMPC/DMPS membranes the protein adopts a rigid β-structure with small amplitude motions. It strongly binds to the bilayer surface and does not penetrate into the acyl chain region leaving the ^{2}H quadrupolar splitting of the fatty acid chains unchanged. Furthermore, a reduction of the ^{31}P NMR chemical shift anisotropy indicates a perturbation of the electronic environment of the phosphate head groups that is introduced by tau K19. Accordingly, raising the pH value or decreasing the content of negatively charged phospholipids is believed to lower the membrane binding since the interaction with tau K19 is mostly driven by electrostatic interactions as shown by changes in the chemical shift for the ^{13}C-methylated lysine side chains.

In DMPS membranes, K19 adopts a different conformational state that is characterized by a higher content of random coil and α-helix structure (Fig. **9**). This state could be similar to the micelle-bound form of tau K19. Along with the observed structural change a redistribution of the protein into the acyl chain region of the bilayer occurs, which is indicated by a decrease of the lipid ^{2}H order parameter profile and causes membrane disruption as seen by an immediate vesicle leakage. This observation is quite surprising because of the highly charged and polar nature of tau K19. There are no obvious hydrophobic patches in the tau sequence that would support membrane penetration. However, a membrane-associated α-helix can lead to a reduction in the partitioning free enthalpy of each peptide bond by 0.5 kcal/mol due to the formation of a stable intramolecular hydrogen bond [55]. Thus, a membrane penetration for short helical patches of K19 could be possible. In that case, both mechanisms *i.e.* membrane binding and secondary structure formation could facilitate one another.

The preference of forming helical intermediate structures during the aggregation process has been found for other amyloidogenic and antimicrobial peptides as well [38]. Depending on the relative peptide-to-lipid concentration, Aβ [86–88], IAPP [89–91] and α-synuclein [92–94] have been shown to shift to an α-helix structure upon membrane binding, which then further proceeds into fibril formation. The anchoring of aggregation-prone peptides to the membrane surface will enhance the local protein concentration, which favors switching to a β-structure and eventually seeding of protein fibrillization. A similar role of a transiently populated helical state of tau K19 could be imagined as well. On the other hand, a helical conformation was not found for K19 in DMPC/DMPS vesicles, which have a physiologically more realistic content of acidic phospholipids. It is possible that the DMPC/DMPS membrane favors a conversion process of an initially helical structure similar to that seen for DMPS. Alternatively, it may be that in the DMPC/DMPS context tau K19 maintains and possibly extends those regions with β-structure, which are already adopted by the soluble protein. Contacts with the bilayer surface may further stabilize the protein structure and can assist interactions between neighboring tau molecules, which could stabilize and explain the observed β-structure.

A second characteristic that tau may share with other amyloidogenic proteins is the ability to disrupt the membrane barrier function. A channel activity was seen for Aβ [95,96], IAPP [97], α-synuclein [98], polyglutamine [99] and prion-derived peptides [100] which is a strong argument for a pore formation by those proteins. In addition a membrane thinning and disintegrating effect simultaneous to fibril growth is discussed for IAPP as well [101,102]. In our cases the rapid kinetics of vesicle leakage strongly argues for a pore formation by tau K19. Since within the time span of leakage no tau fibrils were observed, fibrillization seems not a necessary factor for membrane disruption but rather a monomeric or oligomeric species has to be considered the disruptive species.

Thus, the question of the type of β-structure of K19 in its particular membrane environment arises. Several experimental findings in this study argue against a fibril structure of tau K19 in the presence of DMPC/DMPS membranes. First, no increase in the ThT fluorescence was observed when incubating the protein together with DMPC/DMPS or POPC/POPS liposomes for several days at 37 °C. Secondly, there was no change in the isotropic chemical shifts as a function of the protein–lipid ratio, even at a very high dilution of one protein per 250 lipid molecules. If aggregation had occurred at high protein concentrations, structural changes had likely been caused during that process. Finally, no additional cross peaks in the PDSD spectrum were observed when the experiment was carried out at a longer mixing time of 500 ms. Further correlations could arise from long range couplings *e.g.* between valine and leucine that could indicate a compact monomeric or oligomeric structure. However, contacts might also occur only between amino acids of the same type and hence may be missed in the spectrum unless individual residues could be resolved. Therefore, structural conclusions should not be made on the basis of missing cross-peaks alone.

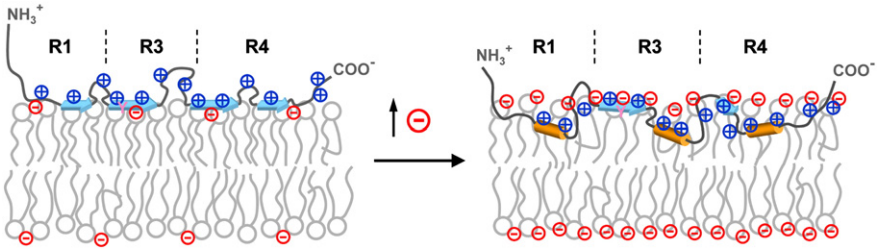

Fig. 9. Proposed structural model of tau K19 in complex with phospholipid membranes that is consistent with the structural constraints obtained from solid-state NMR experiments. Tau K19 adopts a rigid β-structure (blue) with small amplitude motions and is bound to the water membrane interface. In PS membranes K19 can undergo a conformational change towards random coil and α-helix (orange) in certain parts of the protein accompanied by a redistribution into the acyl chain region of the bilayer.

Currently, our data do not provide information regarding long-range interactions between structural elements within membrane-bound tau K19 or between different tau molecules. Apart from a monomeric species, another possible state of membrane-bound tau K19, that is consistent with our data, are tau oligomers. Those complexes possess a significant amount of β-structure but are insensitive to ThT or Congo red, consistent with our observations in DMPC/DMPS. Recently, tau oligomers have emerged as the pathogenic species in tauopathies and were hypothesized as possible mediators of Aβ toxicity in AD [103]. It could be speculated if tau oligomers could execute their cell toxic potential by perturbing the barrier function of the cell membrane *e.g.* by a perforation of the membrane as suggested by our observations of vesicle leakage. Therefore, further analysis is needed to clarify the intra- as well as intermolecular topology of membrane-bound tau K19 and to assess its relevance for tau aggregation and toxicity in AD.

5. Conclusion

The given study provides the first insights into the structure of the membrane-bound state of tau K19. The protein was shown to have a certain propensity towards zwitterionic membranes, which is much increased in the presence of negatively charged lipids. An interaction between lipid headgroups and lysine sidechains of the protein could be observed. In PC/PS mixtures, a predominantly β-sheet-like secondary structure of tau K19 at the membrane surface has been found. The membrane senses the binding of the protein mostly in the headgroup region as detected by ^{31}P NMR spectroscopy. In contrast, no significant alterations of the membrane packing have been observed. In a purely negatively charged membrane, also α-helical secondary structure elements have been found. Those conformational changes were associated with a deeper penetration of tau K19 into the membrane. A significant alteration of the membrane structure was shown by a decrease in the ^{2}H lipid chain order parameter and by tau's membrane permeabilizing potency for DMPS vesicles. In both membrane environments, the secondary structure elements are relatively rigid showing little conformational flexibility. Our results support a potential role of phospholipid membranes for the physiological and pathological functions of tau.

Supplementary data related to this article can be found online at doi:10.1016/j.bbamem.2012.03.019.

Acknowledgements

G.K. is grateful for a grant by the Stiftung Stipendien-Fonds der Chemischen Industrie. The study was supported by a grant from the Deutsche Forschungsgemeinschaft (Transregio-SFB 102, A6).

References

[1] E.H. Koo, P.T. Lansbury, J.W. Kelly, Amyloid diseases: abnormal protein aggregation in neurodegeneration, Proc. Natl. Acad. Sci. U. S. A. 96 (1999) 9989–9990.
[2] L.C. Walker, H. LeVine, The cerebral proteopathies: neurodegenerative disorders of protein conformation and assembly, Mol. Neurobiol. 21 (2000) 83–95.
[3] D.J. Selkoe, D. Schenk, Alzheimer's disease: molecular understanding predicts amyloid-based therapeutics, Annu. Rev. Pharmacol. Toxicol. 43 (2003) 545–584.
[4] I. Grundke-Iqbal, K. Iqbal, M. Quinlan, Y.C. Tung, M.S. Zaidi, H.M. Wisniewski, Microtubule-associated protein tau: a component of Alzheimer paired helical filaments, J. Biol. Chem. 261 (1986) 6084–6089.
[5] K.S. Kosik, C.L. Joachim, D.J. Selkoe, Microtubule-associated protein τ (tau) is a major antigenic component of paired helical filaments in Alzheimer disease, Proc. Natl. Acad. Sci. U. S. A. 83 (1986) 4044–4048.
[6] T. Gomez-Isla, J.L. Price, D.W. McKeel Jr., J.C. Morris, J.H. Growdon, B.T. Hyman, Profound loss of layer II entorhinal cortex neurons occurs in very mild Alzheimer's disease, J. Neurosci. 16 (1996) 4491–4500.
[7] N. Ghoshal, F. Garcia-Sierra, J. Wuu, S. Leurgans, D.A. Bennett, R.W. Berry, L.I. Binder, Tau conformational changes correspond to impairments of episodic memory in mild cognitive impairment and Alzheimer's disease, Exp. Neurol. 177 (2002) 475–493.
[8] N.S. Honson, J. Kuret, Tau aggregation and toxicity in tauopathic neurodegenerative diseases, J. Alzheimers Dis. 14 (2008) 417–422.
[9] I. Grundke-Iqbal, K. Iqbal, Y.C. Tung, M. Quinlan, H.M. Wisniewski, L.I. Binder, Abnormal phosphorylation of the microtubule-associated protein τ (tau) in Alzheimer cytoskeletal pathology, Proc. Natl. Acad. Sci. U. S. A. 83 (1986) 4913–4917.
[10] M.P. Mazanetz, P.M. Fischer, Untangling tau hyperphosphorylation in drug design for neurodegenerative diseases, Nat. Rev. Drug Discov. 6 (2007) 464–479.
[11] M. Goedert, R. Jakes, M.G. Spillantini, M. Hasegawa, M.J. Smith, R.A. Crowther, Assembly of microtubule-associated protein tau into Alzheimer-like filaments induced by sulphated glycosaminoglycans, Nature 383 (1996) 550–553.
[12] P. Friedhoff, A. Schneider, E.M. Mandelkow, E. Mandelkow, Rapid assembly of Alzheimer-like paired helical filaments from microtubule-associated protein tau monitored by fluorescence in solution, Biochemistry 37 (1998) 10223–10230.
[13] T. Kampers, P. Friedhoff, J. Biernat, E.M. Mandelkow, E. Mandelkow, RNA stimulates aggregation of microtubule-associated protein tau into Alzheimer-like paired helical filaments, FEBS Lett. 399 (1996) 344–349.
[14] D.M. Wilson, L.I. Binder, Free fatty acids stimulate the polymerization of tau and amyloid β peptides. *In vitro* evidence for a common effector of pathogenesis in Alzheimer's disease, Am. J. Pathol. 150 (1997) 2181–2195.
[15] M.E. King, V. Ahuja, L.I. Binder, J. Kuret, Ligand dependent tau filament formation: implications for Alzheimer's disease progression, Biochemistry 38 (1999) 14851–14859.
[16] C.N. Chirita, M. Necula, J. Kuret, Anionic micelles and vesicles induce tau fibrillization *in vitro*, J. Biol. Chem. 278 (2003) 25644–25650.
[17] P. Poorkaj, T.D. Bird, E. Wijsman, E. Nemens, R.M. Garruto, L. Anderson, A. Andreadis, W.C. Wiederholt, M. Raskind, G.D. Schellenberg, Tau is a candidate gene for chromosome 17 frontotemporal dementia, Ann. Neurol. 43 (1998) 815–825.
[18] M. Hutton, C.L. Lendon, P. Rizzu, M. Baker, S. Froelich, H. Houlden, S. Pickering-Brown, S. Chakraverty, A. Isaacs, A. Grover, J. Hackett, J. Adamson, S. Lincoln, D. Dickson, P. Davies, R.C. Petersen, M. Stevens, E. de Graaff, E. Wauters, J. van Baren, M. Hillebrand, M. Joosse, J.M. Kwon, P. Nowotny, L.K. Che, J. Norton, J.C. Morris, L.A. Reed, J. Trojanowski, H. Basun, L. Lannfelt, M. Neystat, S. Fahn, F. Dark, T. Tannenberg, P.R. Dodd, N. Hayward, J.B.J. Kwok, P.R. Schofield, A. Andreadis, J. Snowden, D. Craufurd, D. Neary, F. Owen, B.A. Oostra, J. Hardy, A. Goate, J. van Swieten, D. Mann, T. Lynch, P. Heutink, Association of missense and 5′-splice-site mutations in tau with the inherited dementia FTDP-17, Nature 393 (1998) 702–705.
[19] M.G. Spillantini, J.R. Murrell, M. Goedert, M.R. Farlow, A. Klug, B. Ghetti, Mutation in the tau gene in familial multiple system tauopathy with presenile dementia, Proc. Natl. Acad. Sci. U. S. A. 95 (1998) 7737–7741.
[20] C.M. Wischik, M. Novak, P.C. Edwards, A. Klug, W. Tichelaar, R.A. Crowther, Structural characterization of the core of the paired helical filament of Alzheimer-disease, Proc. Natl. Acad. Sci. U. S. A. 85 (1988) 4884–4888.
[21] R. Tycko, Progress towards a molecular-level structural understanding of amyloid fibrils, Curr. Opin. Struct. Biol. 14 (2004) 96–103.
[22] R. Nelson, D. Eisenberg, Recent atomic models of amyloid fibril structure, Curr. Opin. Struct. Biol. 16 (2006) 260–265.
[23] M. von Bergen, P. Friedhoff, J. Biernat, J. Heberle, E.M. Mandelkow, E. Mandelkow, Assembly of tau protein into Alzheimer paired helical filaments depends on a local sequence motif (^{306}VQIVYK^{311}) forming β structure, Proc. Natl. Acad. Sci. U. S. A. 97 (2000) 5129–5134.
[24] J. Berriman, L.C. Serpell, K.A. Oberg, A.L. Fink, M. Goedert, R.A. Crowther, Tau filaments from human brain and from *in vitro* assembly of recombinant protein show cross-β structure, Proc. Natl. Acad. Sci. U. S. A. 100 (2003) 9034–9038.
[25] S. Barghorn, P. Davies, E. Mandelkow, Tau paired helical filaments from Alzheimer's disease brain and assembled *in vitro* are based on β structure in the core domain, Biochemistry 43 (2004) 1694–1703.
[26] O.C. Andronesi, M. von Bergen, J. Biernat, K. Seidel, C. Griesinger, E. Mandelkow, M. Baldus, Characterization of Alzheimer's-like paired helical filaments from the core domain of tau protein using solid-state NMR spectroscopy, J. Am. Chem. Soc. 130 (2008) 5922–5928.
[27] M. von Bergen, S. Barghorn, S.A. Muller, M. Pickhardt, J. Biernat, E.M. Mandelkow, P. Davies, U. Aebi, E. Mandelkow, The core of tau-paired helical filaments studied by scanning transmission electron microscopy and limited proteolysis, Biochemistry 45 (2006) 6446–6457.
[28] J. Kuret, C.N. Chirita, E.E. Congdon, T. Kannanayakal, G.B. Li, M. Necula, H.S. Yin, Q. Zhong, Pathways of tau fibrillization, Biochim. Biophys. Acta 1739 (2005) 167–178.
[29] E. Mandelkow, B.M. von, J. Biernat, E.M. Mandelkow, Structural principles of tau and the paired helical filaments of Alzheimer's disease, Brain Pathol. 17 (2007) 83–90.
[30] M.D. Mukrasch, J. Biernat, B.M. von, C. Griesinger, E. Mandelkow, M. Zweckstetter, Sites of tau important for aggregation populate β-structure and bind to microtubules and polyanions, J. Biol. Chem. 280 (2005) 24978–24986.
[31] D. Eliezer, P. Barre, M. Kobaslija, D. Chan, X. Li, L. Heend, Residual structure in the repeat domain of tau: echoes of microtubule binding and paired helical filament formation, Biochemistry 44 (2005) 1026–1036.
[32] M.D. Mukrasch, P. Markwick, J. Biernat, M. Bergen, P. Bernado, C. Griesinger, E. Mandelkow, M. Zweckstetter, M. Blackledge, Highly populated turn conformations in natively unfolded tau protein identified from residual dipolar couplings and molecular simulation, J. Am. Chem. Soc. 129 (2007) 5235–5243.
[33] P. Barre, D. Eliezer, Folding of the repeat domain of tau upon binding to lipid surfaces, J. Mol. Biol. 362 (2006) 312–326.
[34] M.D. Mukrasch, S. Bibow, J. Korukottu, S. Jeganathan, J. Biernat, C. Griesinger, E. Mandelkow, M. Zweckstetter, Structural polymorphism of 441-residue tau at single residue resolution, PLoS Biol. 7 (2009) e34.

[35] J.A. Hebda, A.D. Miranker, The interplay of catalysis and toxicity by amyloid intermediates on lipid bilayers: insights from type II diabetes, Annu. Rev. Biophys. 38 (2009) 125–152.
[36] C. Aisenbrey, T. Borowik, R. Bystrom, M. Bokvist, F. Lindstrom, H. Misiak, M.A. Sani, G. Grobner, How is protein aggregation in amyloidogenic diseases modulated by biological membranes? Eur. Biophys. J. 37 (2008) 247–255.
[37] A. Relini, O. Cavalleri, R. Rolandi, A. Gliozzi, The two-fold aspect of the interplay of amyloidogenic proteins with lipid membranes, Chem. Phys. Lipids 158 (2009) 1–9.
[38] S.M. Butterfield, H.A. Lashuel, Amyloidogenic protein–membrane interactions: mechanistic insight from model systems, Angew. Chem. Int. Ed. 49 (2010) 5628–5654.
[39] H.A. Lashuel, D. Hartley, B.M. Petre, T. Walz, P.T. Lansbury Jr., Neurodegenerative disease: amyloid pores from pathogenic mutations, Nature 418 (2002) 291.
[40] B.L. Kagan, R. Azimov, R. Azimova, Amyloid peptide channels, J. Membr. Biol. 202 (2004) 1–10.
[41] A. Quist, I. Doudevski, H. Lin, R. Azimova, D. Ng, B. Frangione, B. Kagan, J. Ghiso, R. Lal, Amyloid ion channels: a common structural link for protein-misfolding disease, Proc. Natl. Acad. Sci. U. S. A. 102 (2005) 10427–10432.
[42] H.A. Lashuel, P.T. Lansbury Jr., Are amyloid diseases caused by protein aggregates that mimic bacterial pore-forming toxins? Q. Rev. Biophys. 39 (2006) 167–201.
[43] R. Brandt, J. Leger, G. Lee, Interaction of tau with the neural plasma membrane mediated by tau's amino-terminal projection domain, J. Cell Biol. 131 (1995) 1327–1340.
[44] M. Arrasate, M. Perez, J. Avila, Tau dephosphorylation at tau-1 site correlates with its association to cell membrane, Neurochem. Res. 25 (2000) 43–50.
[45] T. Maas, J. Eidenmüller, R. Brandt, Interaction of tau with the neural membrane cortex is regulated by phosphorylation at sites that are modified in paired helical filaments, J. Biol. Chem. 275 (2000) 15733–15740.
[46] E.G. Gray, M. Paula-Barbosa, A. Roher, Alzheimer's disease: paired helical filaments and cytomembranes, Neuropathol. Appl. Neurobiol. 13 (1987) 91–110.
[47] M. Galvan, J.P. David, A. Delacourte, J. Luna, R. Mena, Sequence of neurofibrillary changes in aging and Alzheimer's disease: a confocal study with phospho-tau antibody, AD2, J. Alzheimers Dis. 3 (2001) 417–425.
[48] S.J. Opella, F.M. Marassi, Structure determination of membrane proteins by NMR spectroscopy, Chem. Rev. 104 (2004) 3587–3606.
[49] D. Huster, Investigations of the structure and dynamics of membrane-associated peptides by magic angle spinning NMR, Prog. Nucl. Magn. Reson. Spectrosc. 46 (2005) 79–107.
[50] G.E. Means, R.E. Feeney, Reductive alkylation of amino groups in proteins, Biochemistry 7 (1968) 2192–2201.
[51] M.J. Hope, M.B. Bally, G. Webb, P.R. Cullis, Production of large unilamellar vesicles by a rapid extrusion procedure: characterization of size distribution, trapped volume and ability to maintain a membrane potential, Biochim. Biophys. Acta 812 (1985) 55–65.
[52] C.H. Huang, Studies on phosphatidylcholine vesicles: formation and physical characteristics, Biochemistry 8 (1969) 344–352.
[53] P.S. Chen, T.Y. Toribara, H. Warner, Microdetermination of phosphorus, Anal. Chem. 28 (1956) 1756–1758.
[54] A.S. Ladokhin, S. Jayasinghe, S.H. White, How to measure and analyze tryptophan fluorescence in membranes properly, and why bother? Anal. Biochem. 285 (2000) 235–245.
[55] S.H. White, W.C. Wimley, Membrane protein folding and stability: physical principles, Annu. Rev. Biophys. Biomol. Struct. 28 (1999) 319–365.
[56] H. Naiki, K. Higuchi, M. Hosokawa, T. Takeda, Fluorometric determination of amyloid fibrils *in vitro* using the fluorescent dye, thioflavine T, Anal. Biochem. 177 (1989) 244–249.
[57] S.W. Provencher, J. Glockner, Estimation of globular protein secondary structure from circular dichroism, Biochemistry 20 (1981) 33–37.
[58] W.C. Johnson, Analyzing protein circular dichroism spectra for accurate secondary structures, Proteins 35 (1999) 307–312.
[59] N. Sreerama, R.W. Woody, A self-consistent method for the analysis of protein secondary structure from circular dichroism, Anal. Biochem. 209 (1993) 32–44.
[60] M.A. Mccabe, S.R. Wassall, Fast-Fourier-transform dePaking, J. Magn. Reson. 106 (1995) 80–82.
[61] M. Lafleur, B. Fine, E. Sternin, P.R. Cullis, M. Bloom, Smoothed orientational order profile of lipid bilayers by ^{2}H-nuclear magnetic resonance, Biophys. J. 56 (1989) 1037–1041.
[62] D. Huster, K. Arnold, K. Gawrisch, Influence of docosahexaenoic acid and cholesterol on lateral lipid organization in phospholipid mixtures, Biochemistry 37 (1998) 17299–17308.
[63] J. Schleucher, M. Schwendinger, M. Sattler, P. Schmidt, O. Schedletzky, S.J. Glaser, O.W. Sorensen, C. Griesinger, A general enhancement scheme in heteronuclear multidimensional NMR employing pulsed field gradients, J. Biomol. NMR 4 (1994) 301–306.
[64] A.E. Bennett, C.M. Rienstra, M. Auger, K.V. Lakshmi, R.G. Griffin, Heteronuclear decoupling in rotating solids, J. Chem. Phys. 103 (1995) 6951–6958.
[65] N.M. Szeverenyi, M.J. Sullivan, G.E. Maciel, Observation of spin exchange by two-dimensional fourier transform ^{13}C cross polarization magic angle spinning, J. Magn. Reson. 47 (1982) 462–475.
[66] C.W.B. Lee, R.G. Griffin, Two-dimensional ^{1}H/^{13}C heteronuclear chemical shift correlation spectroscopy of lipid bilayers, Biophys. J. 55 (1989) 355–358.
[67] D. Huster, K. Arnold, K. Gawrisch, Investigation of lipid organization in biological membranes by two-dimensional nuclear overhauser enhancement spectroscopy, J. Phys. Chem. 103 (1999) 243–251.
[68] M.G. Munowitz, R.G. Griffin, G. Bodenhausen, T.H. Huang, Two-dimensional rotational spin-echo nuclear magnetic resonance in solids: correlation of chemical shift and dipolar interactions, J. Am. Chem. Soc. 103 (1981) 2529–2533.
[69] A. Bielecki, A.C. Kolbert, M.H. Levitt, Frequency-switched pulse sequences: homonuclear decoupling and dilute spin NMR in solids, Chem. Phys. Lett. 155 (1989) 341–346.
[70] P. Barre, O. Zschornig, K. Arnold, D. Huster, Structural and dynamical changes of the bindin B18 peptide upon binding to lipid membranes. A solid-state NMR study, Biochemistry 42 (2003) 8377–8386.
[71] K. Wells, A.A. Farooqui, L. Liss, L.A. Horrocks, Neural membrane phospholipids in Alzheimer disease, Neurochem. Res. 20 (1995) 1329–1333.
[72] A.A. Farooqui, S.I. Rapoport, L.A. Horrocks, Membrane phospholipid alterations in Alzheimer's disease: deficiency of ethanolamine plasmalogens, Neurochem. Res. 22 (1997) 523–527.
[73] J.F. Nagle, Area lipid of bilayers from NMR, Biophys. J. 64 (1993) 1476–1481.
[74] D.S. Wishart, B.D. Sykes, F.M. Richards, Relationship between nuclear magnetic resonance chemical shift and protein secondary structure, J. Mol. Biol. 222 (1991) 311–333.
[75] D.S. Wishart, B.D. Sykes, Chemical shifts as a tool for structure determination, Methods Enzymol. 239 (1994) 363–392.
[76] S. Spera, A. Bax, Empirical correlation between protein backbone conformation and Cα and Cβ ^{13}C nuclear magnetic resonance chemical shifts, J. Am. Chem. Soc. 113 (1991) 5490–5492.
[77] K. Wagner, A.G. Beck-Sickinger, D. Huster, Structural investigations of a human calcitonin-derived carrier peptide in a membrane environment by solid-state NMR, Biochemistry 43 (2004) 12459–12468.
[78] C.X. Gong, F. Liu, I. Grundke-Iqbal, K. Iqbal, Post-translational modifications of tau protein in Alzheimer's disease, J. Neural Transm. 112 (2005) 813–838.
[79] J.K. Andersen, Oxidative stress in neurodegeneration: cause or consequence? Nat. Med. 10 (2004) S18–S25 (Suppl.).
[80] C.C. Mailliot, J.Q. Trojanowski, J.M. Souza, H. Ischiropoulos, Impaired tau protein function following nitration-induced oxidative stress *in vitro* and *in vivo*, Neurobiol. Aging 23 (2002) S415.
[81] R. Mena, P.C. Edwards, C.R. Harrington, E.B. Mukaetova-Ladinska, C.M. Wischik, Staging the pathological assembly of truncated tau protein into paired helical filaments in Alzheimer's disease, Acta Neuropathol. 91 (1996) 633–641.
[82] H.A. Scheidt, I. Morgado, S. Rothemund, D. Huster, Dynamics of amyloid β fibrils revealed by solid-state NMR, J. Biol. Chem. 287 (2012) 2017–2021.
[83] A. Abraha, N. Ghoshal, T.C. Gamblin, V. Cryns, R.W. Berry, J. Kuret, L.I. Binder, C-terminal inhibition of tau assembly *in vitro* and in Alzheimer's disease, J. Cell Sci. 113 (Pt 21) (2000) 3737–3745.
[84] D.L. Minor Jr., P.S. Kim, Measurement of the β-sheet-forming propensities of amino acids, Nature 367 (1994) 660–663.
[85] C.K. Smith, J.M. Withka, L. Regan, A thermodynamic scale for the β-sheet forming tendencies of the amino acids, Biochemistry 33 (1994) 5510–5517.
[86] T.G. Fletcher, D.A. Keire, The interaction of beta-amyloid protein fragment (12–28) with lipid environments, Protein Sci. 6 (1997) 666–675.
[87] H. Shao, S. Jao, K. Ma, M.G. Zagorski, Solution structures of micelle-bound amyloid β-(1–40) and β-(1–42) peptides of Alzheimer's disease, J. Mol. Biol. 285 (1999) 755–773.
[88] P.K. Mandal, J.W. Pettegrew, Alzheimer's disease: soluble oligomeric Aβ(1–40) peptide in membrane mimic environment from solution NMR and circular dichroism studies, Neurochem. Res. 29 (2004) 2267–2272.
[89] J.D. Knight, J.A. Hebda, A.D. Miranker, Conserved and cooperative assembly of membrane-bound α-helical states of islet amyloid polypeptide, Biochemistry 45 (2006) 9496–9508.
[90] M. Apostolidou, S.A. Jayasinghe, R. Langen, Structure of α-helical membrane-bound human islet amyloid polypeptide and its implications for membrane-mediated misfolding, J. Biol. Chem. 283 (2008) 17205–17210.
[91] J.A. Williamson, J.P. Loria, A.D. Miranker, Helix stabilization precedes aqueous and bilayer-catalyzed fiber formation in islet amyloid polypeptide, J. Mol. Biol. 393 (2009) 383–396.
[92] T.S. Ulmer, A. Bax, N.B. Cole, R.L. Nussbaum, Structure and dynamics of micelle-bound human α-synuclein, J. Biol. Chem. 280 (2005) 9595–9603.
[93] C.C. Jao, B.G. Hegde, J. Chen, I.S. Haworth, R. Langen, Structure of membrane-bound α-synuclein from site-directed spin labeling and computational refinement, Proc. Natl. Acad. Sci. U. S. A. 105 (2008) 19666–19671.
[94] E.R. Georgieva, T.F. Ramlall, P.P. Borbat, J.H. Freed, D. Eliezer, Membrane-bound α-synuclein forms an extended helix: long-distance pulsed ESR measurements using vesicles, bicelles, and rodlike micelles, J. Am. Chem. Soc. 130 (2008) 12856–12857.
[95] N. Arispe, E. Rojas, H.B. Pollard, Alzheimer disease amyloid β protein forms calcium channels in bilayer membranes: blockade by tromethamine and aluminum, Proc. Natl. Acad. Sci. U. S. A. 90 (1993) 567–571.
[96] H.B. Pollard, E. Rojas, N. Arispe, A new hypothesis for the mechanism of amyloid toxicity, based on the calcium channel activity of amyloid β protein (AβP) in phospholipid bilayer membranes, Ann. N. Y. Acad. Sci. 695 (1993) 165–168.
[97] T.A. Mirzabekov, M.C. Lin, B.L. Kagan, Pore formation by the cytotoxic islet amyloid peptide amylin, J. Biol. Chem. 271 (1996) 1988–1992.
[98] H.Y. Kim, M.K. Cho, A. Kumar, E. Maier, C. Siebenhaar, S. Becker, C.O. Fernandez, H.A. Lashuel, R. Benz, A. Lange, M. Zweckstetter, Structural properties of pore-forming oligomers of α-synuclein, J. Am. Chem. Soc. 131 (2009) 17482–17489.

[99] H. Monoi, S. Futaki, S. Kugimiya, H. Minakata, K. Yoshihara, Poly-L-glutamine forms cation channels: relevance to the pathogenesis of the polyglutamine diseases, Biophys. J. 78 (2000) 2892–2899.
[100] J.I. Kourie, A. Culverson, Prion peptide fragment PrP[106–126] forms distinct cation channel types, J. Neurosci. Res. 62 (2000) 120–133.
[101] E. Sparr, M.F. Engel, D.V. Sakharov, M. Sprong, J. Jacobs, B. de Kruijff, J.W. Höppener, J.A. Killian, Islet amyloid polypeptide-induced membrane leakage involves uptake of lipids by forming amyloid fibers, FEBS Lett. 577 (2004) 117–120.
[102] M.F. Engel, L. Khemtémourian, C.C. Kleijer, H.J. Meeldijk, J. Jacobs, A.J. Verkleij, B. de Kruijff, J.A. Killian, J.W. Höppener, Membrane damage by human islet amyloid polypeptide through fibril growth at the membrane, Proc. Natl. Acad. Sci. U. S. A. 105 (2008) 6033–6038.
[103] C.A. Lasagna-Reeves, D.L. Castillo-Carranza, M.J. Guerrero-Munoz, G.R. Jackson, R. Kayed, Preparation and characterization of neurotoxic tau oligomers, Biochemistry 49 (2010) 10039–10041.
[104] http://www.bmrb.wisc.edu/index.html.